



HAL
open science

Kinetics of CrPV and HCV IRES-mediated eukaryotic translation using single molecule fluorescence microscopy

Olivier Bugaud, Nathalie Barbier, H el ene Chommy, Nicolas Fiszman, Antoine Le Gall, David Dulin, Matthieu Saguy, Nathalie Westbrook, Karen Perronet, Olivier Namy

► To cite this version:

Olivier Bugaud, Nathalie Barbier, H el ene Chommy, Nicolas Fiszman, Antoine Le Gall, et al.. Kinetics of CrPV and HCV IRES-mediated eukaryotic translation using single molecule fluorescence microscopy. *RNA*, 2017, 23 (11), pp.1626-1635. 10.1261/rna.061523.117 . hal-01575997

HAL Id: hal-01575997

<https://iogs.hal.science/hal-01575997v1>

Submitted on 22 Aug 2017

HAL is a multi-disciplinary open access archive for the deposit and dissemination of scientific research documents, whether they are published or not. The documents may come from teaching and research institutions in France or abroad, or from public or private research centers.

L'archive ouverte pluridisciplinaire **HAL**, est destin ee au d ep ot et  a la diffusion de documents scientifiques de niveau recherche, publi es ou non,  emanant des  tablissements d'enseignement et de recherche fran ais ou  trangers, des laboratoires publics ou priv es.

Kinetics of CrPV and HCV IRES-mediated eukaryotic translation using single molecule fluorescence microscopy

Olivier Bugaud¹, Nathalie Barbier², H el ene Chommy^{1,2}, Nicolas Fiszman², Antoine Le Gall², David Dulin², Matthieu Saguy¹, Nathalie Westbrook², Karen Perronet^{2,*} and Olivier Namy^{1,*}

¹ Institute for Integrative Biology of the Cell (I2BC), CEA, CNRS, Universit  Paris-Sud, Universit  Paris-Saclay, France

² Laboratoire Charles Fabry, Institut d'Optique, CNRS, Universit  Paris-Saclay, 91127 Palaiseau, France

* To whom correspondence should be addressed. Tel: +33 1 69 15 50 51; Fax: +33 1 69 15 72 96; Email: Olivier.namy@i2bc.paris-saclay.fr. Correspondence may also be addressed to Karen Perronet. Tel: +33 1 64 53 33 48 ; Fax +33 1 64 53 31 01 ; Karen.perronet@institutoptique.fr.

The authors wish it to be known that, in their opinion, the first two authors should be regarded as joint First Authors.

Present Address: Le Gall Antoine, Centre de Biochimie Structurale, CNRS and INSERM, 29 rue de Navacelles, 34090, Montpellier, France
Dulin David, IZKF - Interdisciplinary Center for Clinical Research, Friedrich-Alexander-University Erlangen-Nuremberg (FAU), Germany

ABSTRACT

Protein synthesis is a complex multi-step process involving many factors that need to interact in a coordinated manner to properly translate the messenger RNA. As translating ribosomes cannot be synchronized over many elongation cycles, single molecule studies have been introduced to bring a deeper understanding of prokaryotic translation dynamics. Extending this approach to eukaryotic translation is very appealing, but initiation and specific labelling of the ribosomes are much more complicated. Here we use a non-canonical translation initiation based on internal ribosome entry sites (IRES) and we monitor the passage of individual, unmodified mammalian ribosomes at specific fluorescent milestones along mRNA. We explore initiation by two types of IRES, the intergenic IRES of Cricket Paralysis virus (CrPV) and the hepatitis C (HCV) IRES, and show that they both strongly limit the rate of the first elongation steps compared to the following ones suggesting that those first elongation cycles do not correspond to a canonical elongation. This new system opens the possibility to study both IRES-mediated initiation and elongation kinetics of eukaryotic translation and will undoubtedly be a valuable tool to investigate the role of translation machinery modifications in human diseases.

INTRODUCTION

During translation, the ribosome decodes the mRNA sequence in discrete codon steps; tRNAs move from the A- and P-sites to the P- and E-sites, which are universally conserved in all kingdoms of life (Valle et al. 2003). Although the ribosome inner structure is well conserved, eukaryotic translation

remains more complicated. The structures of the 80S eukaryotic ribosome, and of its small (40S) and large (60S) subunits, have been elucidated only very recently and show extended rRNA segments together with several eukaryote-specific proteins (Ben-Shem et al. 2011). It is thought that these changes compared to prokaryotic ribosomes are for regulatory purposes to interconnect the ribosome with several biological pathways (Klinge et al. 2012).

The dynamics of translation are difficult to study using traditional biochemical and biophysical tools because it is a highly stochastic process, involving multiple steps and factors. Single molecule techniques circumvent the need to synchronize the process and have become more and more popular over the last ten years to study prokaryotic translation kinetics (Cornish et al. 2008; Marshall et al. 2008; Katranidis et al. 2009; Chen et al. 2013; Rosenblum et al. 2013; Chen et al. 2014). Many of them involve specific labelling of the prokaryotic ribosome, which has been achieved thanks to the knowledge of its atomic structure (Yusupov et al. 2001). Recently, Puglisi's group reported the labelling of eukaryotic ribosomes, either by hybridization of labelled oligonucleotides (Petrov and Puglisi 2010; Fuchs et al. 2015) or by labelling eS25 protein (Petrov and Puglisi 2010; Fuchs et al. 2015), without affecting ribosome assembly capacity. However, fluorescently labelling the ribosome, the tRNA substrates or the elongation factors may modify their behaviour in an unpredictable way. Furthermore, most single molecule fluorescence techniques are limited to a very low concentration of labels in solution (a few 10 nM typ.), which can also dramatically modify the kinetics of the process (Uemura et al. 2010). Although several clever approaches have been developed to study eukaryotic translation by single molecule FRET (Ferguson et al. 2015), all of them rely on modifying either the ribosome itself or translational factors like tRNA to attach a fluorescent dye. An approach with unmodified translational components is of great interest to analyse eukaryotic translation dynamics as shown by the recent *in vivo* quantification of translational speed (Morisaki et al. 2016; Murray et al. 2016; Wang et al. 2016; Wu et al. 2016).

Here, we report on eukaryotic translation kinetics starting from an internal ribosome entry site (IRES) mediated initiation and on going over several elongation cycles using single-molecule total internal reflection fluorescence microscopy (sm-TIRFM) with unmodified mammalian translation machinery, ensuring that labelling will not denature translation. Only the mRNA is labelled through the annealing of short fluorescent RNA probes (see Figure 1A), which can be detached by the ribosome because of its helicase activity, as shown previously (Takyar et al. 2005).

Translation initiation usually requires the correct positioning of the aminoacyl-tRNA in the ribosomal P-site. In eukaryotes this is achieved by a large number of initiation factors allowing the 40S together with the ternary complex (eIF2-tRNA-GTP) to scan the 5' part of the mRNA until the initiator tRNA is correctly base paired with the start codon in the P-site. Viruses have developed numerous translational strategies to express viral proteins or to divert host translation machinery for their own benefit (Firth and Brierley 2012). Among them, internal initiation is commonly used to bypass the requirement of eIF4 complex (Thompson 2012; Wang et al. 2013). IRES are grouped into

four categories that differ with respect to their secondary structure, the translation initiation factors they require, and whether or not they recruit the ribosome upstream of the initiation codon or directly at it.

To initiate translation we use first the intergenic region cricket paralysis virus IRES (hereafter simply referred to as CrPV IRES). This is a type IV IRES, enabling the ribosome to translate its mRNA independently of any cellular initiation factors (Wilson et al. 2000). A large number of genetic, biochemical and structural studies have contributed to characterize this IRES (Wilson et al. 2000; Deniz et al. 2009; Fernandez et al. 2014). Since the first description of the CrPV IRES, it has been thought that it would enable binding of the ribosome directly in an active state by mimicking tRNA/mRNA interaction in the P-site, ready to accommodate tRNA^{Ala} in the A-site (Costantino et al. 2008; Au and Jan 2012). However, recent work has demonstrated that the first binding step occurs one codon upstream than previously anticipated (as represented in Figure 1B). Accommodating the first alanine codon in the A-site requires a translocation step involving eEF2 (Fernandez et al. 2014; Muhs et al. 2015). A second unconventional translocation cycle may possibly occur before the IRES fully leaves the ribosome (Petrov et al. 2016). How the ribosome can accommodate a structure as large as an IRES is an intriguing question, especially in terms of translocation. In the presence of the IRES, eEF2 leads to the formation of an unstable intermediate state that is determined by the entry of tRNA in the A-site either in the 0 or +1 frame (Petrov et al. 2016).

Although the dynamics of the 40S and 80S subunits recruitment to the CrPV-IRES has been recently described (Petrov et al. 2016), how the very first cycles kinetics compare to the subsequent elongation cycles, especially in a homogeneous system, remains unknown. Using a single molecule strategy, we were able to quantify the elongation rate of an unmodified single mammalian ribosome and calculate the kinetics of translation during several elongation steps. This work confirms that the first one, or possibly two translocation steps are unusual and inefficient in the presence of the CrPV-IRES, with a characteristic time almost 30 times longer than for a classical elongation cycle.

To investigate the applicability of this method to any mRNA with an IRES, we also performed experiments with the Hepatitis C Virus (HCV) IRES. We show that this IRES also slows down the first cycle. This methodology opens the possibility of studying the behaviour of different IRES as well as the kinetics of eukaryotic translation in conditions where changes in translation are suspected to be responsible for genetic diseases or cancers (Stumpf and Ruggero 2011; Reschke et al. 2013).

MATERIAL AND METHODS

Plasmids and oligonucleotides

pCH1 contains the CrPV IGR IRES (coordinates 6028 to 6219 from the viral mRNA) downstream of the SP6 promoter as well as a region where the chimeric biotinylated DNA/2' O-allyl modified RNA oligonucleotide (Namy et al. 2006) binds upstream an HpaI site. The plasmid pCH2 is identical to

pCH1 except that in pCH2, the coding sequence of the PB1 gene (from pPS0 plasmid) (Somogyi et al. 1993) without stop codon was inserted into the HpaI site. This allowed us to extend the initial coding sequence to make the polypeptide visible in gel during *in vitro* translation assay. The pCH3 plasmid also derives from pCH1 with the insertion of the sequence TCTACTGCTGAACTCGCT at the HpaI site to insert the UP-primer binding site. The DOWN-primer site has been chosen to have a melting temperature compatible with the UP-primer. The plasmid pCH4 derives from pCH3 with a deletion of the IRES named Δ IRES in the manuscript. The plasmid pCH5 derives from pCH3 with 3 additional codons inserted upstream from the UP-primer to increase the distance between the IRES and the UP-primer. pHCV is a pUC19 derivative plasmid containing the HCV-type 1b IRES followed by the first 6 codons of the core protein coding sequence (NCBI accession number AJ238799 from nucleotide 1 to 360). All other features are identical to pCH1.

RNA oligonucleotides coupled to an ATTO fluorophore were synthesized by Eurogentec. The UP-primer (5'- AAAGAGUUCAGCAGU-3') is identical to the oligonucleotide H12 from (Takyar et al. 2005), except for the 3 A at the 5' end used to space the fluorescent label from the hybridized region. The label is either ATTO647N or ATTO565, excited in the red and in the green part of the spectrum respectively. The associated nomenclature is thus R-UP-primer and G-UP-primer respectively. The DOWN-primer sequence is 5'-ATTO565-AAACUUCUCGAGCUU-3'. This primer binds downstream from the UP-primer. To create MUTUP and MUTDOWN binding sites have been mutated by replacing the original sequence by its complementary to prevent binding of the primers.

In vitro transcription

Plasmids were linearized with the appropriate restriction enzyme (KpnI or XhoI) and transcribed *in vitro* with SP6 RNA polymerase (Promega). RNA is purified using RNA-Spin columns (Roche).

Purification of ribosomal subunits

Ribosomal subunits were prepared from nuclease-treated rabbit reticulocyte lysate (RRL; Promega). A 1ml RRL was mixed with 3ml buffer A (20mM Hepes pH 7.8, 150mM K(OAc), 6mM Mg(OAc)₂ and 2mM dithiothreitol (DTT)) and incubated with 1mM puromycin (Sigma) for 10 min at 4°C and then for 10 min at 37°C. Ribosomal subunits were isolated by centrifugation of this suspension through a 3ml 20% sucrose cushion in buffer A for 4 h at 4°C and 44,000 rpm, using a Beckman TLA110 rotor. Pellets were resuspended in buffer A to a concentration of 12 A₂₆₀ U/ml.

Non-denaturing gel mobility shifts

Conditions for native gel shift assays are the following: pCH2-derived mRNA (500nM) was incubated with 100nM R-UP-primer in a 10 μ L reaction in buffer B (20mM Tris pH 7.8, 5mM MgCl₂, 5mM DTT and 0.25mM ATP) for 5min at 68°C, 5min at 37°C and 5min in ice. mRNA/oligonucleotide complexes were diluted 20 times in buffer C (20mM Hepes pH 7.8, 100mM K(OAc), 2.5mM Mg(OAc)₂, 2mM DTT and 0.25mM spermidine). This complex (5nM) is incubated in buffer C with an increasing concentration of ribosomal subunits, from 0 to 40nM, at 37°C for 10min. For controls, the

mRNA/oligonucleotide complex (5nM) was incubated with 30nM ribosomal subunits and with an increasing concentration of either competitor or non-competitor RNA from 0 to 100nM. Competitor RNA only contains the CrPV IRES sequence. Yeast tRNA (Sigma) is used as a non-competitor RNA. Gel shifts were performed in 0.8% (w/v) agarose gels in THM buffer (66mM Hepes, 34mM Tris, 2.5mM MgCl₂, final pH 7.5) at room temperature. Gel-mobility shifts were analyzed by fluorescence scanning with a 633nm laser and a filter 670BP30 (Typhoon, GE Healthcare).

Single-molecule experiments

A home-built objective-based TIRF microscope was used. ATTO-647N and ATTO-565-labeled molecules were excited using a 640-nm laser diode or a 532-nm diode-pumped solid-state laser (both Oxixius). Fluorescence emission was collected by a 1.45 NA 60x oil-immersion objective (PlanApo, Olympus) and imaged onto an electron-multiplying charged coupled device (CCD) camera (iXon+897 Andor) at 100 or 200-ms exposure. The excitation and detection of ATTO-647N and ATTO-565 fluorescence were alternated using home-built electronics. The two lasers were reflected on the same dichroic mirror (Chroma z532/633rpc) and a motorized filter wheel was used to choose the appropriate emission filter (resp. Chroma HQ665lp and Semrock FF01-580/60). A laboratory-built microscope-based focus drift correction was used to keep the focus during the whole experiment. Cellular extract delivery was achieved using a modified syringe pump (Harvard Apparatus) (dead time 2-3s). In RRL, for an exposure time of 200 ms every 5 s, the lifetime before photobleaching of ATTO647N (resp. ATTO565) was $\tau_R = 85 \pm 16$ s ($\tau_G = 38 \pm 6$ s).

In vitro translation on a surface

The mRNA from pCH3, pCH4, pCH5 and pHCV plasmids (0.5 μ M) were annealed to the chimeric biotinylated DNA/2' O-allyl modified RNA oligonucleotide (0.5 μ M) and 2 μ M fluorescent labeled oligonucleotides in a 10 μ l reaction in 0.5x ligase buffer (NEB) for 5min at 68°C, 5min at 37°C and 5min at 4°C. The mRNA/oligonucleotides complexes were diluted 100 times in buffer E (20mM Hepes pH 7.8, 100mM Na(OAc), 100mM K(OAc), 2.5mM Mg(OAc)₂, 2mM DTT and 0.25mM spermidine). The mRNA/primers complexes were further diluted in buffer E to 0.8nM. For the experiments where the 80S ribosomes were pre-assembled on CrPV IRES, 24nM ribosomal subunits were added to this solution. The reaction was incubated at 37°C for 10 min prior to injection in the flow-cell and allowed to bind for 10min to the biotin-PEG-derivatized glass coverslip. The chamber was flushed with buffer E before injection of 25 μ l RRL mix (17.5 μ l RRL, 6 μ l H₂O, 20U SUPERase In (Ambion) and 0.5 μ l of amino acid – Cys mix provided) previously incubated at 30°C for 10min. Control experiments were carried out in the presence of 355 μ M cycloheximide (Euromedex) in each solution. When the RRL reached the excitation area, data acquisition was launched. Every 5 seconds (unless otherwise stated), two images were acquired, first in the red channel and 500ms later in the green one.

Data analysis

For each color, analysis was performed on individual spots, provided that they were diffraction limited and that they were present in the first two images and disappeared abruptly (after one frame) during

the movie. Errors bars on the primer departure probability curves $D(t)$ and on the fitting parameters were obtained by a bootstrapping procedure (Press et al. 1995). For each set of N_0 experimental data points, 1000 samples of N_0 bootstrapped points were computed. The same analysis procedure was performed on each bootstrapped sample: each one was fitted, leading to the average fitting parameters and their standard deviations given in the text.

RESULTS

An mRNA was labelled with two small RNA fluorescent probes along its coding sequence and to a biotinylated one at its 5' end. Depending on the experiments, a single 80S ribosome, purified from RRL was bound to this mRNA or not. The mRNA was then attached to a coverslip through its 5' end (Figure 1A). This coverslip formed the bottom part of a microfluidic chamber. Translation started when total rabbit reticulocyte lysate (RRL), which contains all the factors needed to perform translation, was injected into the chamber. Translation kinetics data was obtained by measuring the departure times out of the evanescent wave for each probe. Ribosomal mRNA entry channel can only admit a single strand RNA (Yusupova et al. 2001), so the ribosome must unfold mRNA secondary structures (Takyar et al. 2005; Qu et al. 2011) to continue translation until it reaches the stop codon. Small RNA probes have been previously used to map this helicase activity (Takyar et al. 2005). We selected two probes linked to two spectrally distinct fluorophores (ATTO647N for R-primers and ATTO565 for G-primers, see an example in Figure 1B). Based on the work by (Takyar et al. 2005) and the fact that canonical ribosomal footprints from eukaryotes and prokaryotes are both 28nt in length, we assume that eukaryotic helicase activity is located at the same position as for prokaryotic ribosomes (Martens et al. 2015). We conclude that 5 elongation cycles are needed to fully detach the UP-(+5)-primer, as shown in Fig.1B. This system allows us to synchronize the departure of the downstream probe (DOWN-primer) using the upstream probe (UP-primer) departure as a reference.

The mRNA labelling is sequence-specific

Both primers efficiently bind to the same mRNA as shown in Figure 1C. We were able to dual label ~80% of the mRNA from pCH2 or pCH4 with R-UP-(+5) and G-DOWN-(+14) in our annealing conditions. To further demonstrate the absence of primers mis-pairing we created mRNAs with mutations on either the UP or the DOWN primer binding sites, called resp. MUTUP and MUTDOWN mRNAs hereafter. The mRNAs should then not be able to attach to either the UP or the DOWN labeled primers. We then performed the hybridization with the UP and DOWN primers, with the rest of the experiment in the same conditions as with the non-mutated mRNAs. In our single-molecule experiment, as expected, we observed 0.1 to 1% spots in the color of the primer corresponding to the mutated site compared to the number of spots in the other color, where the mRNA region was not mutated (Fig.1D). These very few remaining spots correspond most likely to inhomogeneities in the background fluorescence from the coverslip or its surface chemistry used to attach the mRNAs. Furthermore, we observe almost no colocalized spots: 0% green spots when the red primer site is

mutated, and 2% when the green primer site is mutated, due to more background noise in the green channel. This demonstrates that primers specifically bind their targets without mis-pairing.

The CrPV-IRES supports ribosome binding in the presence of the labelled primers

One major difficulty to set up such a system was the reconstitution of the translation initiation step in vitro. This step involves more than 40 factors in eukaryotes, several of them being modified post-translationally (Aitken and Lorsch 2012). To circumvent this difficulty we used first the CrPV IRES intergenic region to initiate translation. This IRES, which enables binding of the 80S ribosome in the absence of initiation factors and initiator tRNA, has been very well characterized, both functionally and structurally (Jan and Sarnow 2002; Pestova et al. 2004; Spahn et al. 2004; Petrov et al. 2016). We first demonstrated that despite the binding of the UP-(+5)-primer close to the ribosome assembly region on the mRNA, CrPV IRES was still able to specifically recruit the 40S subunit (or possibly directly the 80S ribosome) from purified ribosomes (Petrov et al. 2016) (Figure 2). This demonstrated that CrPV-IRES supports ribosome binding in the presence of primers positioned as in our single molecule experiments.

The ribosome efficiently translates mRNAs with CrPV IRES in the microfluidic chamber

We first used mRNAs with CrPV-IRES, preincubated with 80S ribosomes. We observed the individual initiation complexes using a home-built objective-based two-color total-internal reflection fluorescence microscope, allowing localisation of dual labelled mRNAs in real time during translation. We first plotted the total number N of remaining R-UP-(+5)-primers versus time, normalized by the initial number of R-UP-(+5)-primers N_0 (see Figure 3A) (same for G-DOWN-(+14)-primer, data not shown). The total number of analyzed data points is given in Table 1. In order to check that the observed departure phenomenon was not a pure photobleaching effect, well known for organic dyes, we recorded the same movie on a different area of the sample, 30 min after RRL injection, i.e. long after translation was over. The photobleaching curve $N^{\text{pb}}(t)$ (Figure 3A, grey curve) decreases to only $79 \pm 6\%$ after 50 s, which is much higher than the $49 \pm 7\%$ observed in the translation test, $N^{\text{exp}}(t)$ (Figure 3A, red curve). This indicates that most departures in the first 50 seconds after the RRL injection cannot be attributed to photobleaching.

Other biological activities, such as RNase could also explain fluorophore departures. However, the fact that there is no mRNA degradation is demonstrated by the observation of a non-illuminated area after RRL injection in presence of an mRNA with no IRES. As there was no laser excitation, photobleaching cannot account for fluorophore departure in this area and the absence of IRES prevents initiation to occur. We observed many spots in the non-illuminated area, same as before injection of the RRL. This indicates that there was no mRNA degradation during the experiment.

To identify the departures due to translation, we performed two additional control experiments. First, we preincubated RRL with cycloheximide. This antibiotic binds to the ribosomal E-site and blocks translation after 2 cycles (Pestova and Hellen 2003). Adding cycloheximide clearly slowed down

fluorophore departures but did not prevent them completely (Figure 3A, blue curve). In a second control experiment, we used an mRNA without the IRES sequence (Δ IRES mRNA) to prevent translation initiation. The corresponding curve $N^{\Delta\text{IRES}}(t)$ (Figure 3A, purple curve) is very close to the cycloheximide control indicating that indeed in both situations translation is inhibited. We believe that the few remaining departures in both controls were due to the flow during injection and to the salinity difference when injecting the RRL, although we reduced it by optimizing the salt concentration of the initial buffer. In any case, the departure rate of the R-UP-(+5)-primer is clearly significantly higher with IRES and no cycloheximide (Figure 3A, red curve), and we conclude that this increase in the departure rate is due to translating ribosomes.

mRNAs with HCV IRES are also efficiently translated

To further confirm these results we performed the same experiment using an mRNA carrying the HCV IRES with and without a stop codon before the R-DOWN fluorescent primer (Figure 3D). The presence of the stop codon prevents the departure of R-DOWN primers, in the same extend as the absence of the IRES. These results performed with a different mRNA demonstrate that translation is responsible for primer departure.

Determination of the ribosome speed during elongation

We then focused on the R-UP-(+5) and G-DOWN-(+14)-primers, hybridized on a CrPV-IRES mRNA, that were co-localized on the first red and green images. We calculated the histograms H^{exp} and $H^{\Delta\text{IRES}}$ of the departures of both primers as a function of the difference $t_{\text{DOWN}} - t_{\text{UP}}$, with and without the IRES sequence. The times t_{UP} and t_{DOWN} correspond to the departures of R-UP-(+5) and G-DOWN-(+14) from a given mRNA strand. The histograms H^{exp} and $H^{\Delta\text{IRES}}$ were normalized by the initial number of co-localized spots. The difference $H^{\text{trans}} = H^{\text{exp}} - H^{\Delta\text{IRES}}$ is plotted in figure 3B and a Gaussian fit shows a maximum at 12.5 ± 2.1 s. Thus, on average, G-DOWN-(+14) departs from a given mRNA strand 12.5 s after R-UP-(+5). Because the lifetime before photobleaching of the red fluorophore is three times larger than that of the green one, departures due to photobleaching would on average occur in the inverse order. Thus, the fact that this histogram is centred at $t_{\text{DOWN}} > t_{\text{UP}}$ is yet another confirmation that we observed translation. As 9 elongation cycles are needed between the two fluorophore departures, we conclude that one elongation cycle takes an average of 1.4 ± 0.2 s.

CrPV IRES-bound ribosomes are responsible for the translation events observed in single molecule experiments

Because the cell extract used for the single-molecule experiments contains ribosomes, we performed control experiments without pre-incubating purified 80S ribosomes on CrPV IRES mRNAs to quantify the contribution of free RRL ribosomes to the signal observed in the experiments. In both cases, the same mRNA was used. We analysed the departure times for each primer. Figure 3C shows the derivatives $D^{\text{trans}}(t) = d(N^{\text{exp}}(t)/N^{\Delta\text{IRES}}(t))$, which represent the probability for the UP-(+5) probe to disappear at time t in two cases: with pre-incubated purified ribosomes (red curve) or without (black curve). The area under each curve in Fig 3C corresponds to the fraction of probe carrying mRNAs

that were translated. This translation efficiency is much larger (50%) in the experiment with pre-incubation of the 80S than without (10%). This indicates that hardly 10% of the mRNAs were translated without pre incubation of the ribosomes. So free ribosomes are not efficient to initiate translation at the CrPV IRES in the RRL. Actually this is in agreement with previous a paper from Pestova's group (Pestova et al. 2004). These experiments showed that the presence of initiation factors inhibits subunit joining at the CrPV IRES.

Ribosomes present in RRL efficiently translate HCV-IRES mRNAs

To confirm that the type of CrPV-IRES prevents efficient initiation of the ribosome in RRL, we used HCV-IRES. This IRES is a type III IRES that only requires eIF3 and eIF2 as initiation factors and has been shown to be very efficient in RRL (Borman et al. 1995). Using this IRES we show that translation efficiency is 30% without ribosome pre-incubation (Fig 3.E).

Both HCV and CrPV IRES poise the first translational steps

The primer departure due to translation occurs when the ribosome has performed n elongation cycles ($n=5$ for R-UP-(+5)). If all the elongation cycles were identical, the fitting function for $D^{\text{trans}}(t)$ would be a gamma law $p(t) = \frac{t^{n-1} \exp(-t/t_{el})}{t_{el}^n (n-1)!}$ with t_{el} the characteristic time for one elongation cycle. However, this function, for $n=5$, does not fit our experimental data, indicating that one time parameter is not sufficient to describe the dynamics observed. We considered that the ribosome translation is well described by a rapid phase corresponding to the first part of the $D^{\text{trans}}(t)$ curve, and a slow one, corresponding to the tail of $D^{\text{trans}}(t)$. The simplest fitting function with two time parameters that could describe these data is the convolution of one slow event happening with an exponential probability of characteristic duration t_0 , and a rapid phase described by an exponential probability of characteristic duration t_1 :

$$D^{\text{fit}}(t) = \frac{A}{t_0 - t_1} \left(e^{-t/t_0} - e^{-t/t_1} \right)$$

where, A corresponds to the fraction of translated mRNAs.

For CrPV IRES we performed the same fitting procedure to the $D^{\text{trans}}(t)$ curves for different primers, hybridized at different locations on the mRNA, and included a bootstrapping process to evaluate the mean value and the error bars on the fitting parameters A , t_0 and t_1 . In addition to the R-UP-(+5) and G-DOWN-(+14) primers, we tested an mRNA from pCH5 with 9 additional nucleotides upstream from the R-UP-primer hybridization site. In this situation, the ribosome must translate 8 codons (instead of 5 previously) before the R-UP-(+8)-primer departure (same R-UP-primer). The results of all the fits are summarized in Table 2. t_0 describes a slow phase lasting typically 40s, independently of the primer. t_1 corresponds to the fast phase. Within the error bars, its value is proportional to $n-1$ or $n-2$. Furthermore, the elongation time t_{el} obtained by dividing t_1 by $n-1$ or $n-2$ is consistent with the elongation time of 1.4 ± 0.2 s previously measured between the R-UP-(+5) and G-DOWN-(+14)-primer departures. To test whether melting the double strand formed by the primer and the mRNA

slowed down the ribosome, we added a third fitting time parameter and found it to be consistent with zero within our error bars. We conclude that unzipping the primer has a negligible effect on our measured elongation time. The fact that the time t_0 for the slow phase is independent of the primer location and that it is longer than the time interval between the two primer departures proves that it is not due to the unzipping of the RNA probes but corresponds to an event that occurs only between the translation starting point and the UP-primer departure. Using the same fitting procedure for HCV IRES we obtained $t_0 = 29 \pm 4$ s, indicating that both IRES-mediated translations display the same kinetics scheme (compare Figure 3C and 3E).

DISCUSSION

Our approach allows quantification of elongation speed in two ways. Purified and pre-incubated ribosomes translate at a rate of 1.4 ± 0.2 s per codon. This value is slightly slower than the one obtained by ribosome profiling approach (0.2 s per codon) (Ingolia et al. 2012). However with non-purified ribosomes, the translation rate increases 3 fold (0.5 ± 0.2 s per codon), which is in good agreement with the kinetics already obtained *in vivo* (Morisaki et al. 2016; Wang et al. 2016; Wu et al. 2016; Yan et al. 2016). Although the kinetics of initiation has recently been addressed in a heterogeneous cell-free system (Zhang et al. 2016), the consequences of the IRES-dependent initiation for the elongation cycles have never been evaluated in an unmodified translation system. Interestingly comparison between both systems gives different results. Zhang et al observed 4 slow translocation cycles whereas our data fit with only 2 slow translocations that could correspond to the slowest cycles described by Zhang et al. (see Table 2). One may suspect that heterogeneity in the translation system leads to kinetics issues. Indeed they describe four very slow steps (between 80 and 200 s for one translocation) and even the faster cycles are at least 30 fold slower than the translocation speed obtained *in vivo* (0.1 translocation/ second vs 3 translocations/ second respectively). Such values cannot represent physiological speed of translation and reflect problems due to the heterogeneity of their system (shrimp ribosomes with yeast elongation factors in the presence of *E. coli* tRNA). Actually, it is true that CrPV IRES is well known to support translation initiation using various ribosomes (yeast, human, shrimp) (Thompson et al. 2001; Spahn et al. 2004), however this does not imply that initiation kinetics is conserved in all these artificial systems. Using the CrPV IRES we measured the speed of eukaryotic ribosomes and were able to identify two characteristic times: a very long time (40s) that corresponds to the first (or the first plus the second) translocation step, and a short time (1.4s) for all remaining translocations. This translocation time is in good agreement with recent *in vivo* experiments that indicated a ribosome translocation rate around 3 ± 1 amino acids per second (Morisaki et al. 2016; Wang et al. 2016; Wu et al. 2016; Yan et al. 2016).

Our data support the model proposed by the Ramakrishnan's team (Fernandez et al. 2014; Murray et al. 2016). They observed by high-resolution cryoEM the exact position of the intergenic CrPV IRES in interaction with the ribosome and showed that this IRES enables the ribosome to assemble one codon upstream than what was previously anticipated. Moreover, they showed that eEF2 is able to

translocate the PKI part of the IRES (mimicking the tRNA in the A-site) from the A- to the P-site, allowing the A-site to accept the next cognate tRNA. Our results indicate that the translocation of PKI from the A- to the P- site is a rate-limiting event (almost 30 times longer than a canonical elongation cycle). As one may anticipate this translocation is very unusual, because the ribosome has to deal with a very large secondary structure. Once this first step has occurred, the second elongation cycle takes place with a tRNA in the A-site and the IRES bound between P- and E-sites. This second elongation cycle is probably also kinetically slow (see Table 2), however our data indicate that once these translocations are over, all further translocations occur at the same speed. This suggests that during the next translocation step, IRES is not anymore a limiting factor. Due to time resolution limits we cannot exclude that with PKI in the P-site and a cognate tRNA in the A-site, the translocation occurs at a normal speed due to a quick release of the PKI from the ribosome (Figure 4).

It has been shown that HCV IRES assembles an 80S ribosome that is poised at the initiator codon (Filbin et al. 2013). This takes place through the interaction of part of the IRES with the β -hairpin of the ribosomal protein uS7 and with the N-terminal helix–turn–helix motif of eS25 (Quade et al. 2015). Both IRES share common features; in particular they both interact with uS7 as described by cryo-EM studies (Spahn et al. 2004; Boehringer et al. 2005; Filbin et al. 2013). However, unlike CrPV, the HCV IRES requires several initiation factors (Lukavsky 2009). A recent cryoEM study revealed that the swine fever virus IRES (similar to HCV IRES) displaces the core of eIF3 from its position on the 40S subunit (Hashem et al. 2013). This binding would reduce eIF3 availability to form a canonical 43S pre-initiation complex. From these data it seems clear that both IRESs induce similar conformational changes in the ribosome despite utilizing distinct mechanisms for translation initiation. In both cases IRES represent a hindrance to ribosome movement and explain our observation that both CrPV and HCV IRES strongly slow down ribosome translocation during the first elongation cycles. One may postulate this is a general feature of IRES initiation.

More generally, our results demonstrate that the system we have developed is well suited to study translation kinetics at the single molecule level during multiple elongation cycles. It can be applied to numerous translational questions. For example, it is now well established that the translation machinery is a target for deregulation in diseases such as cancers (Stumpf and Ruggero 2011; Marcel et al. 2013). The ability to quantify translation kinetics in such environments will provide great improvements in the understanding of how the translational machinery is involved in these pathologies.

ACKNOWLEDGEMENT

The authors would like to thank D. Fourmy, S. Yoshizawa, J.D. Puglisi and B.S. Cooperman for fruitful discussions.

FUNDING

This work was supported by Centre National de la Recherche Scientifique (CNRS) (Programme Interdisciplinaire du CNRS, Interface Physique-Chimie-Biologie, soutien à la prise de risque to K.P.), PRES Univer'Sud (2010-08 to O.N.), the Region Ile-de-France in the framework of C'Nano IdF, the nanoscience competence center of Paris Region (CINERIB to K.P.), Agence Nationale de la Recherche (ANR) (Ribodyn ANR-10-BLAN-1510 to K.P, Ribometh ANR-13-BSV8-0012-02 to O.N), a Fondation pour la Recherche Médicale fellowship (to H.C and O.B), a CNRS PhD fellowship (to N.F.), an IDI 2014 fellowship funded by the IDEX Paris-Saclay ANR-11-IDEX-003-02 (to N.B.) and a ANR post-doctoral fellowship (to M.S). Funding for open access charge: (Agence Nationale de la Recherche/ANR-13-BSV8-0012-02)

REFERENCES

- Aitken CE, Lorsch JR. 2012. A mechanistic overview of translation initiation in eukaryotes. *Nat Struct Mol Biol* **19**: 568-576.
- Au HH, Jan E. 2012. Insights into factorless translational initiation by the tRNA-like pseudoknot domain of a viral IRES. *PLoS One* **7**: e51477.
- Ben-Shem A, Garreau de Loubresse N, Melnikov S, Jenner L, Yusupova G, Yusupov M. 2011. The structure of the eukaryotic ribosome at 3.0 Å resolution. *Science* **334**: 1524-1529.
- Boehringer D, Thermann R, Ostareck-Lederer A, Lewis JD, Stark H. 2005. Structure of the hepatitis C virus IRES bound to the human 80S ribosome: remodeling of the HCV IRES. *Structure* **13**: 1695-1706.
- Borman AM, Bailly JL, Girard M, Kean KM. 1995. Picornavirus internal ribosome entry segments: comparison of translation efficiency and the requirements for optimal internal initiation of translation in vitro. *Nucleic Acids Res* **23**: 3656-3663.
- Chen C, Zhang H, Broitman SL, Reiche M, Farrell I, Cooperman BS, Goldman YE. 2013. Dynamics of translation by single ribosomes through mRNA secondary structures. *Nat Struct Mol Biol* **20**: 582-588.
- Chen J, Petrov A, Johansson M, Tsai A, O'Leary SE, Puglisi JD. 2014. Dynamic pathways of -1 translational frameshifting. *Nature* **512**: 328-332.
- Cornish PV, Ermolenko DN, Noller HF, Ha T. 2008. Spontaneous intersubunit rotation in single ribosomes. *Molecular cell* **30**: 578-588.
- Costantino DA, Pfingsten JS, Rambo RP, Kieft JS. 2008. tRNA-mRNA mimicry drives translation initiation from a viral IRES. *Nat Struct Mol Biol* **15**: 57-64.
- Deniz N, Lenarcic EM, Landry DM, Thompson SR. 2009. Translation initiation factors are not required for Dicistroviridae IRES function in vivo. *RNA* **15**: 932-946.
- Ferguson A, Wang L, Altman RB, Terry DS, Juette MF, Burnett BJ, Alejo JL, Dass RA, Parks MM, Vincent CT et al. 2015. Functional Dynamics within the Human Ribosome Regulate the Rate of Active Protein Synthesis. *Molecular cell* **60**: 475-486.
- Fernandez IS, Bai XC, Murshudov G, Scheres SH, Ramakrishnan V. 2014. Initiation of translation by cricket paralysis virus IRES requires its translocation in the ribosome. *Cell* **157**: 823-831.
- Filbin ME, Vollmar BS, Shi D, Gonen T, Kieft JS. 2013. HCV IRES manipulates the ribosome to promote the switch from translation initiation to elongation. *Nat Struct Mol Biol* **20**: 150-158.
- Firth AE, Brierley I. 2012. Non-canonical translation in RNA viruses. *The Journal of general virology* **93**: 1385-1409.
- Fuchs G, Petrov AN, Marceau CD, Popov LM, Chen J, O'Leary SE, Wang R, Carette JE, Sarnow P, Puglisi JD. 2015. Kinetic pathway of 40S ribosomal subunit recruitment to hepatitis C virus internal ribosome entry site. *Proc Natl Acad Sci U S A* **112**: 319-325.

- Hashem Y, des Georges A, Dhote V, Langlois R, Liao HY, Grassucci RA, Pestova TV, Hellen CU, Frank J. 2013. Hepatitis-C-virus-like internal ribosome entry sites displace eIF3 to gain access to the 40S subunit. *Nature* **503**: 539-543.
- Ingolia NT, Brar GA, Rouskin S, McGeachy AM, Weissman JS. 2012. The ribosome profiling strategy for monitoring translation in vivo by deep sequencing of ribosome-protected mRNA fragments. *Nat Protoc* **7**: 1534-1550.
- Jan E, Sarnow P. 2002. Factorless ribosome assembly on the internal ribosome entry site of cricket paralysis virus. *J Mol Biol* **324**: 889-902.
- Katranidis A, Atta D, Schlesinger R, Nierhaus KH, Choli-Papadopoulou T, Gregor I, Gerrits M, Buldt G, Fitter J. 2009. Fast biosynthesis of GFP molecules: a single-molecule fluorescence study. *Angewandte Chemie* **48**: 1758-1761.
- Klinge S, Voigts-Hoffmann F, Leibundgut M, Ban N. 2012. Atomic structures of the eukaryotic ribosome. *Trends Biochem Sci* **37**: 189-198.
- Lukavsky PJ. 2009. Structure and function of HCV IRES domains. *Virus research* **139**: 166-171.
- Marcel V, Ghayad SE, Belin S, Therizols G, Morel AP, Solano-Gonzalez E, Vendrell JA, Hacot S, Mertani HC, Albaret MA et al. 2013. p53 acts as a safeguard of translational control by regulating fibrillarin and rRNA methylation in cancer. *Cancer Cell* **24**: 318-330.
- Marshall RA, Aitken CE, Dorywalska M, Puglisi JD. 2008. Translation at the single-molecule level. *Annual review of biochemistry* **77**: 177-203.
- Martens AT, Taylor J, Hilser VJ. 2015. Ribosome A and P sites revealed by length analysis of ribosome profiling data. *Nucleic Acids Res* **43**: 3680-3687.
- Morisaki T, Lyon K, DeLuca KF, DeLuca JG, English BP, Zhang Z, Lavis LD, Grimm JB, Viswanathan S, Looger LL et al. 2016. Real-time quantification of single RNA translation dynamics in living cells. *Science* **352**: 1425-1429.
- Muhs M, Hilal T, Mielke T, Skabkin MA, Sanbonmatsu KY, Pestova TV, Spahn CM. 2015. Cryo-EM of ribosomal 80S complexes with termination factors reveals the translocated cricket paralysis virus IRES. *Molecular cell* **57**: 422-432.
- Murray J, Savva CG, Shin BS, Dever TE, Ramakrishnan V, Fernandez IS. 2016. Structural characterization of ribosome recruitment and translocation by type IV IRES. *eLife* **5**.
- Namy O, Moran SJ, Stuart DI, Gilbert RJ, Brierley I. 2006. A mechanical explanation of RNA pseudoknot function in programmed ribosomal frameshifting. *Nature* **441**: 244-247.
- Pestova TV, Hellen CU. 2003. Translation elongation after assembly of ribosomes on the Cricket paralysis virus internal ribosomal entry site without initiation factors or initiator tRNA. *Genes Dev* **17**: 181-186.
- Pestova TV, Lomakin IB, Hellen CU. 2004. Position of the CrPV IRES on the 40S subunit and factor dependence of IRES/80S ribosome assembly. *EMBO Rep* **5**: 906-913.
- Petrov A, Grosely R, Chen J, O'Leary SE, Puglisi JD. 2016. Multiple Parallel Pathways of Translation Initiation on the CrPV IRES. *Molecular cell* **62**: 92-103.
- Petrov A, Puglisi JD. 2010. Site-specific labeling of *Saccharomyces cerevisiae* ribosomes for single-molecule manipulations. *Nucleic Acids Res* **38**: e143.
- Press WH, Teukolsky SA, Vetterling WT, Flannery BP. 1995. *Numerical Recipes in C*. Cambridge University Press New York, NY, USA.
- Qu X, Wen JD, Lancaster L, Noller HF, Bustamante C, Tinoco I, Jr. 2011. The ribosome uses two active mechanisms to unwind messenger RNA during translation. *Nature* **475**: 118-121.
- Quade N, Boehringer D, Leibundgut M, van den Heuvel J, Ban N. 2015. Cryo-EM structure of Hepatitis C virus IRES bound to the human ribosome at 3.9-Å resolution. *Nature communications* **6**: 7646.
- Reschke M, Clohessy JG, Seitzer N, Goldstein DP, Breitkopf SB, Schmolze DB, Ala U, Asara JM, Beck AH, Pandolfi PP. 2013. Characterization and analysis of the composition and dynamics of the Mammalian riboproteome. *Cell Rep* **4**: 1276-1287.

- Rosenblum G, Chen C, Kaur J, Cui X, Zhang H, Asahara H, Chong S, Smilansky Z, Goldman YE, Cooperman BS. 2013. Quantifying elongation rhythm during full-length protein synthesis. *Journal of the American Chemical Society* **135**: 11322-11329.
- Somogyi P, Jenner AJ, Brierley I, Inglis SC. 1993. Ribosomal pausing during translation of an RNA pseudoknot. *Mol Cell Biol* **13**: 6931-6940.
- Spahn CM, Jan E, Mulder A, Grassucci RA, Sarnow P, Frank J. 2004. Cryo-EM visualization of a viral internal ribosome entry site bound to human ribosomes: the IRES functions as an RNA-based translation factor. *Cell* **118**: 465-475.
- Stumpf CR, Ruggero D. 2011. The cancerous translation apparatus. *Curr Opin Genet Dev* **21**: 474-483.
- Takyar S, Hickerson RP, Noller HF. 2005. mRNA helicase activity of the ribosome. *Cell* **120**: 49-58.
- Thompson SR. 2012. Tricks an IRES uses to enslave ribosomes. *Trends Microbiol* **20**: 558-566.
- Thompson SR, Gulyas KD, Sarnow P. 2001. Internal initiation in *Saccharomyces cerevisiae* mediated by an initiator tRNA/eIF2-independent internal ribosome entry site element. *Proc Natl Acad Sci U S A* **98**: 12972-12977.
- Uemura S, Aitken CE, Korlach J, Flusberg BA, Turner SW, Puglisi JD. 2010. Real-time tRNA transit on single translating ribosomes at codon resolution. *Nature* **464**: 1012-1017.
- Valle M, Zavialov A, Sengupta J, Rawat U, Ehrenberg M, Frank J. 2003. Locking and unlocking of ribosomal motions. *Cell* **114**: 123-134.
- Wang C, Han B, Zhou R, Zhuang X. 2016. Real-Time Imaging of Translation on Single mRNA Transcripts in Live Cells. *Cell* **165**: 990-1001.
- Wang QS, Au HH, Jan E. 2013. Methods for studying IRES-mediated translation of positive-strand RNA viruses. *Methods* **59**: 167-179.
- Wilson JE, Pestova TV, Hellen CU, Sarnow P. 2000. Initiation of protein synthesis from the A site of the ribosome. *Cell* **102**: 511-520.
- Wu B, Eliscovich C, Yoon YJ, Singer RH. 2016. Translation dynamics of single mRNAs in live cells and neurons. *Science* **352**: 1430-1435.
- Yan X, Hoek TA, Vale RD, Tanenbaum ME. 2016. Dynamics of Translation of Single mRNA Molecules In Vivo. *Cell* **165**: 976-989.
- Yusupov MM, Yusupova GZ, Baucom A, Lieberman K, Earnest TN, Cate JH, Noller HF. 2001. Crystal structure of the ribosome at 5.5 Å resolution. *Science* **292**: 883-896.
- Yusupova GZ, Yusupov MM, Cate JH, Noller HF. 2001. The path of messenger RNA through the ribosome. *Cell* **106**: 233-241.
- Zhang H, Ng MY, Chen Y, Cooperman BS. 2016. Kinetics of initiating polypeptide elongation in an IRES-dependent system. *eLife* **5**.

TABLE AND FIGURES LEGENDS

Table 1: Values of the initial number N_0 of primers for each experiment, The value indicated in italics represents the total number of departures after 50s, except for the colocalized primers (*) where it is given at the end of the experiment (after 250s).

Table 2: Summary of the results obtained from the fits.

Figure 1. Single ribosome translation assay: design, ribosome location on mRNA, and fluorescent labelling **A)** The mRNA/ribosome complex is attached to a PEG-neutravidin coated coverslip through a biotinylated probe hybridized to the 5' part of the mRNA. mRNA is labelled with the fluorescent probes (UP- and DOWN-primers). **B)** Initial locations of the ribosomal A, P and E sites are indicated. The curved dash line represents the extremity of the ribosome when bound to the IRES. The IRES initiator codon located at the A-site is indicated in red. To prevent any influence of the ATTO-dye on the probes annealing efficiency, 3 uncomplementary nucleotides have been added to the probes (in blue). Dashed lines represent the position of the ribosome extremity for which 100 % of each primer is detached. *** indicates the first codon read by a tRNA after translocation of PKI of the IRES from A to P site. **C)** Zoom on single-molecule TIRFM images of UP-(+5)-R primers (left), DOWN-(+14)-G-primers (center). Overlay (right) shows co-localisation in yellow. Images are background-filtered using imageJ. **D)** Same single-molecule TIRFM images as in C) using a mRNA where the DOWN-primer (top line) or UP-primer (bottom line) binding site sequence is replaced by its complementary sequence. Signal scale is the same for the 2 images of each channel.

Figure 2. Specific binding of the ribosome to the IRES. For each gel shift assay, concentrations of R-(UP)+5-primers, mRNA, and ribosomal subunits (40S and 60S) are indicated. Mobility shifts were visualized using the primer fluorescence as indicated in Material and Methods. **A)** Increasing the concentration of ribosomal subunits induces a gel shift only in the presence of mRNA. The 30nM concentration of ribosomal subunits is selected for further experiments. **B)** Increasing the concentration of a non-specific RNA competitor (tRNA) does not change the gel shift. **C)** Increasing the concentration of a specific but non fluorescent RNA competitor (CrPV IRES) reduces the binding of the ribosomal subunits to the mRNA. Images have been obtained by fluorescence scanning with a 633nm laser and a filter 670BP30 (Typhoon, GE Healthcare). Contrast and brightness have been modified if necessary using Photoshop CS6. These changes have been applied equally across the entire images.

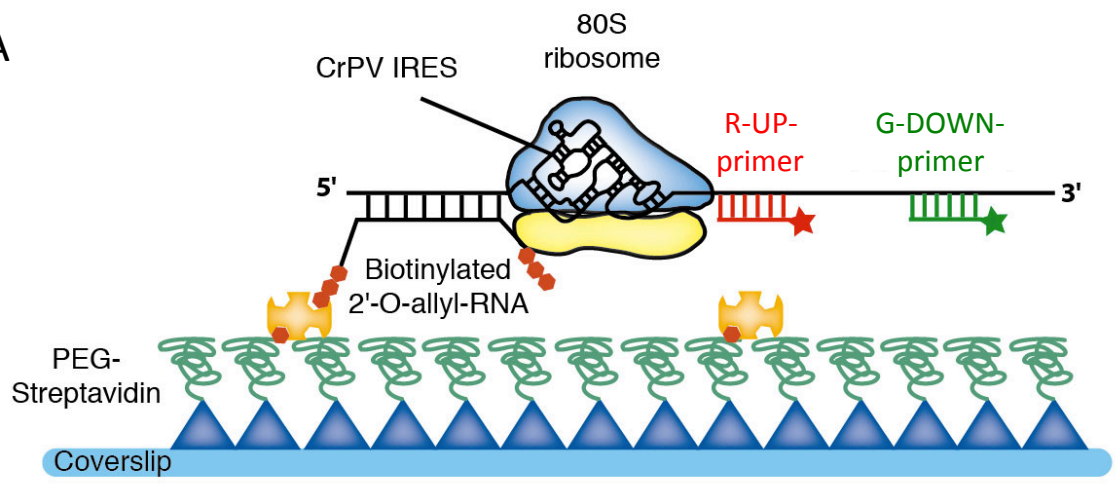
Figure 3. Analysis of the UP- and DOWN- primers departure times on CrPV and HCV IRES mRNAs. **A)** Fraction of remaining R-UP-(+5) primers versus time for the CrPV IRES mediated translation experiment (red), controls using cycloheximide (blue), an mRNA without IRES (purple), and photobleaching (grey). $t=0$ is the RRL arrival time at the imaged area. Errors bars are the standard deviation of all the curves obtained for each image sequence (7 sequences for translation, 6 for Δ IRES control, 3 for cycloheximide control, 12 for photobleaching). **B)** Orange curve: histogram showing the fraction of colocalized spots (in % - Y axis) from which G-DOWN-(+14) and R-UP-(+5) primers depart with a given time interval (in s – X axis). Black curve: Gaussian fit of this histogram. **C)** Fraction of R-UP-(+5) primers disappearing at a given time (red markers), and fit using a two-parameter model (red solid line). Comparison with G-UP-(+5) primers disappearing at a given time (black markers) in a control experiment without 80S pre-incubation, with the corresponding fitting curve (black solid line). All experiments are performed with pre-incubated ribosomes, except for the control in panel C. **D)** Fraction of remaining R-DOWN-(+24) primers versus time for the HCV IRES

mediated translation experiment (red), controls using HCV-IRES mRNA with a STOP codon before DOWN binding site (brown), and an mRNA without IRES (purple). $t=0$ is the RRL arrival time at the imaged area, time between 2 images is 2,5 s. Errors bars are the standard deviation of all the curves obtained for each image sequence (5 sequences for translation, 9 for mRNA with STOP control, 5 for Δ IRES control). **E)** Fraction of R-UP-(+24) primers disappearing at a given time (red markers), and fit using a two-parameter model (red solid line).

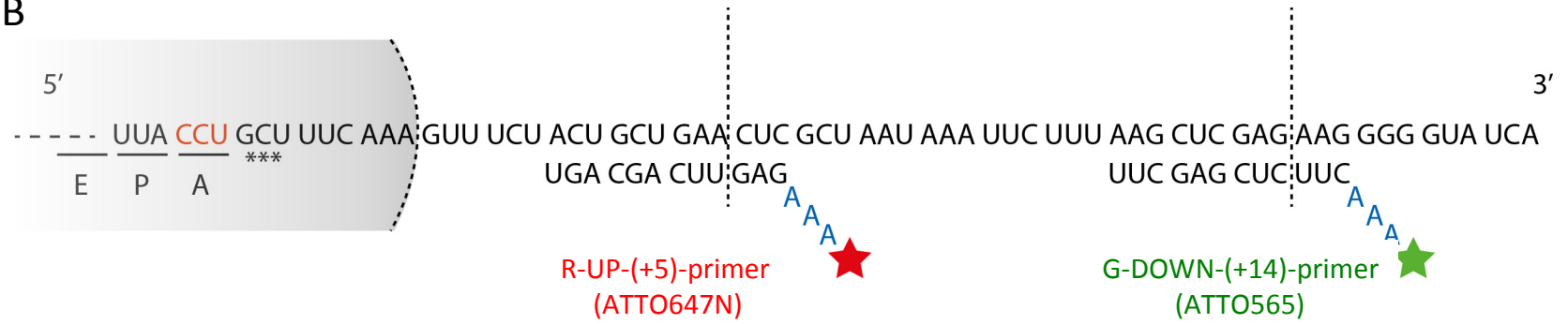
In panels B, C and E, correction was performed using mRNA without IRES and the plotted curves represent the average curves of the bootstrapping procedure described in Material and Methods, with error bars given by the standard deviation of the bootstrapped samples.

Figure 4. Model for first translocation cycles from the CrPV IRES. Translocation of the PKI of the IRES (green part) from A to P sites is a very slow step catalysed by eEF2. The free A-site is mostly filled by a cognate tRNA^{Ala} at the alanine codon (***) (when translation initiates in the 0 frame). From our data we cannot exclude that the next elongation cycle also occurs slowly, due to the presence of the IRES in P and E-sites (down panel). Elongation then resumes at high speed (1.4s). All subsequent steps occur at the same speed indicating that IRES no longer impacts the functioning of the ribosome.

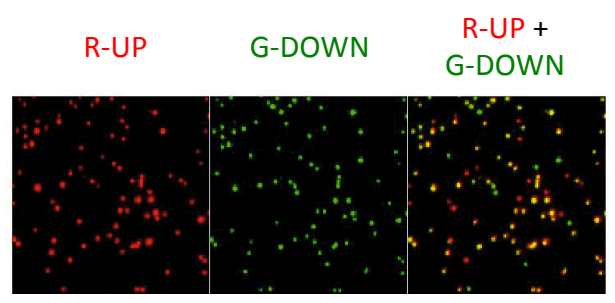
A



B



C



D

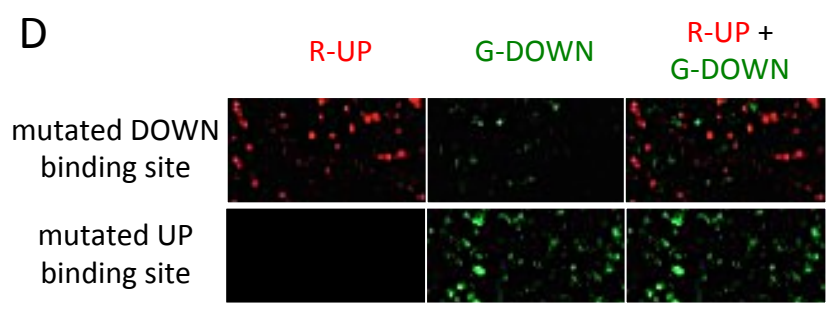
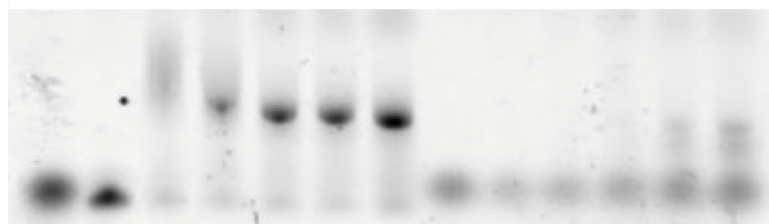


Figure 1

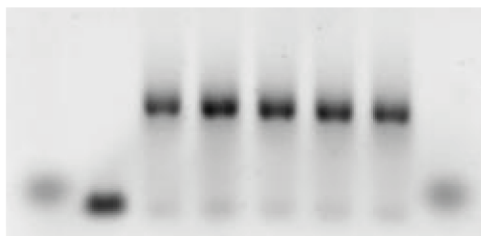
A

_____ 1 _____												nM primer	
_____ 5 _____												nM mRNA	
0	0	5	10	20	30	40	0	5	10	20	30	40	nM 40S + 60S



B

_____ 1 _____												nM primer	
_____ 5 _____												nM mRNA	
_____ 30 _____												nM 40S + 60S	
0	0	0	5	10	50	100	100						nM tRNA



C

_____ 1 _____												nM primer
_____ 5 _____												nM mRNA
_____ 30 _____												nM 40S + 60S
0	5	0	5	10	50	100						nM CrPV IRES

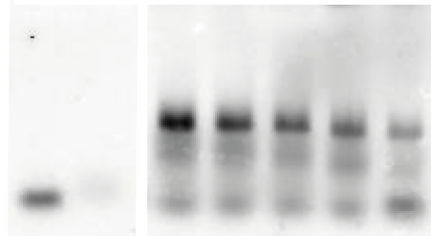


Figure 2

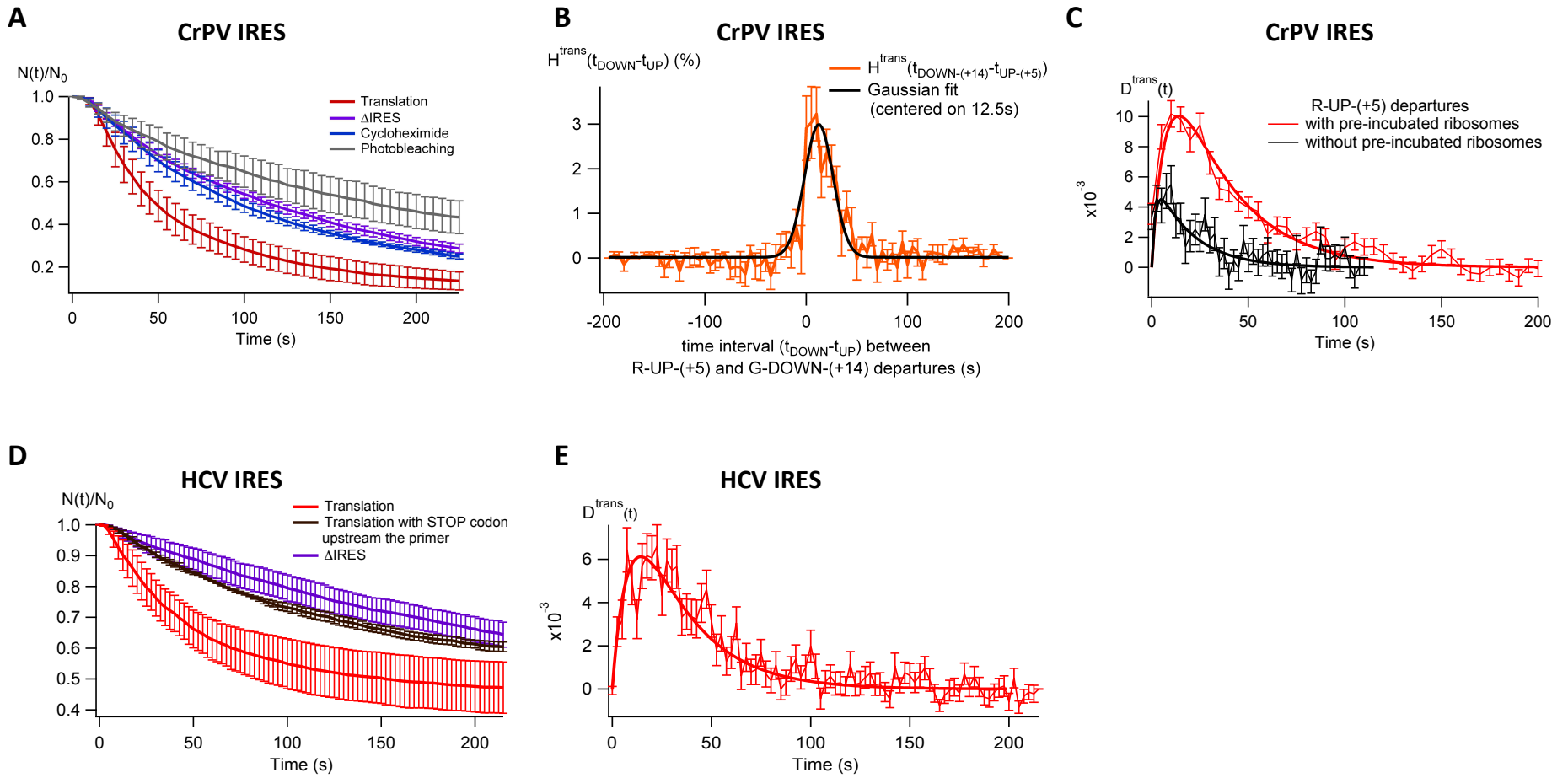


Figure 3

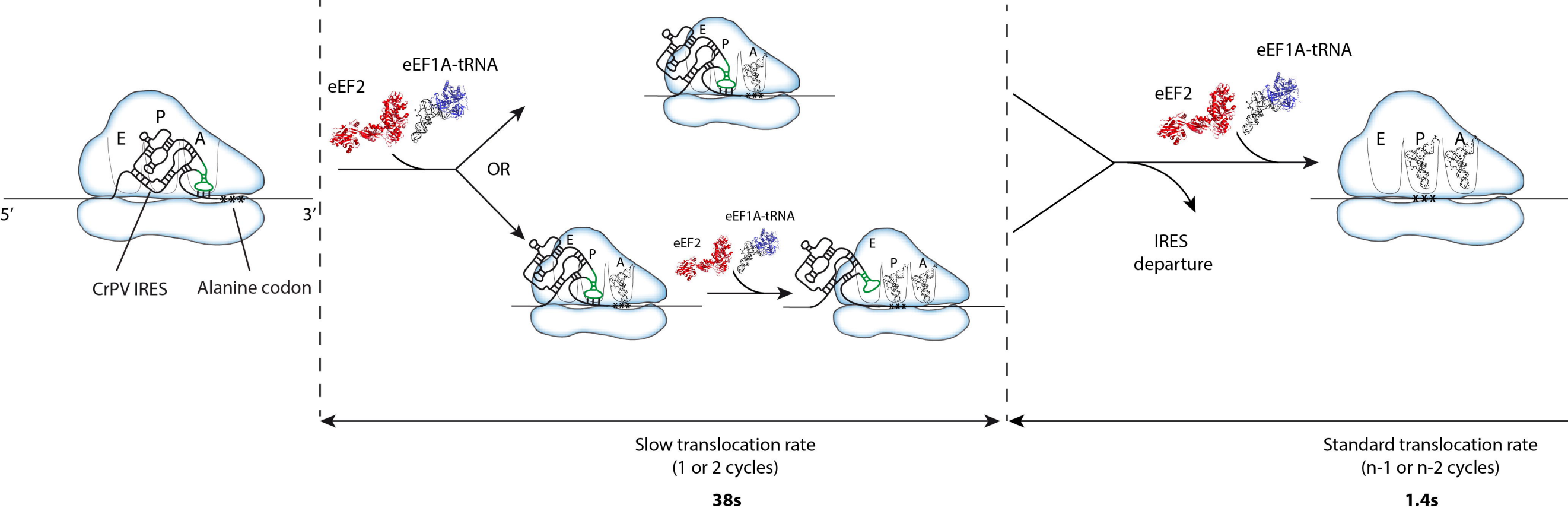


Figure 4

CrPV IRES				
Experiment	Initial number of / (<i>total number of departures after 50 s</i>)			
	R-UP-(+5)	G-DOWN-(+14)	Colocalized primers	R-UP-(+8)
Translation	7112 / (3627)	1754 / (930)	1494 / (651*)	5756 / (3511)
ΔIRES mRNA control	6991 / (1888)	1176 / (396)	646 / (140*)	2905 / (813)
Cycloheximide control	2924 / (877)			
Photobleaching	1486 / (312)			

HCV IRES	
Experiment	Initial number of / (<i>total number of departures after 50 s</i>)
	R-DOWN-(+24)
Translation	4111 / (1398)
ΔIRES mRNA control	4303 / (473)
mRNA with STOP control	8182 / (1309)

Table 1

CrPV IRES			
	R-UP-(+5)	G-DOWN-(+14)	R-UP-(+8)
A (%)	51±1	46±2	72±2
t_0 (s)	38±3	36±10	47±3
t_1 (s)	4.2±0.8	10.4±6.5	7.7±1.0
Hyp. 1 : $t_e/l = t_1/(n-1)$ (s)	1.1±0.2	0.8±0.5	1.1±0.1
Hyp. 2 : $t_e/l = t_1/(n-2)$ (s)	1.4±0.3	0.9±0.5	1.3±0.1
t_e/l (s) from histogram	1.4±0.2		

HCV IRES	
	R-DOWN-(+24)
A (%)	30±1
t_0 (s)	29±4
t_1 (s)	11.6±4.6
$t_e/l = t_1/(n-1)$ (s)	0.5±0.2

Table 2



RNA

A PUBLICATION OF THE RNA SOCIETY

Kinetics of CrPV and HCV IRES-mediated eukaryotic translation using single molecule fluorescence microscopy

Olivier Bugaud, Nathalie Barbier, H  l  ne Chommy, et al.

RNA published online August 2, 2017

P<P	Published online August 2, 2017 in advance of the print journal.
Accepted Manuscript	Peer-reviewed and accepted for publication but not copyedited or typeset; accepted manuscript is likely to differ from the final, published version.
Open Access	Freely available online through the <i>RNA</i> Open Access option.
Creative Commons License	This article, published in <i>RNA</i> , is available under a Creative Commons License (Attribution-NonCommercial 4.0 International), as described at http://creativecommons.org/licenses/by-nc/4.0/ .
Email Alerting Service	Receive free email alerts when new articles cite this article - sign up in the box at the top right corner of the article or click here .



Biofluids too dilute to detect
microRNAs? See what to do.

EXIQON

To subscribe to *RNA* go to:
<http://rnajournal.cshlp.org/subscriptions>
